Structural optimization of pseudorotaxane-forming oligonucleotides for efficient and stable complex formation

Kazumitsu Onizuka[1],*, Takuya Miyashita[1], Tomoko Chikuni[1], Mamiko Ozawa[1], Hiroshi Abe[2] and Fumi Nagatsugi[1],*

[1]Institute of Multidisciplinary Research for Advanced Materials, Tohoku University, 2-1-1 Katahira, Aoba-ku, Sendai, Miyagi 980-8577, Japan and [2]Department of Chemistry, Graduate School of Science, Nagoya University, Furo-cho, Chikusa-ku, Nagoya 464-8602, Japan

ABSTRACT

Interlocked structures, such as rotaxane and catenane, combine both static and dynamic properties. To expand their unique properties into the chemical biology field, a spontaneous formation method of the interlocked structures with the target would be ideal. We have previously developed a pseudorotaxane-forming oligo DNA (prfODN) to spontaneously form topological DNA/RNA architectures. In this study, we report the structural optimization of prfODNs for the efficient and stable complex formation. The optimized prfODNs efficiently formed pseudorotaxane structures with a DNA or RNA target, and the yield for the RNA target reached 85% in 5 min. In addition, the optimized prfODNs could form the pseudorotaxane structure with a smaller ring size and the structure significantly increased the kinetic stability. Furthermore, the catenane structure was successfully formed with the optimized prfODNs to provide the conclusive evidence for the formation of the threaded structure. This information will be valuable for developing new chemical methods using functional nucleic acids for antisense oligo nucleotides and DNA/RNA nanotechnology.

INTRODUCTION

Rotaxane is a molecular architecture consisting of a dumbbell-shaped molecule which is threaded through a molecular ring. This dumbbell-shaped molecular axle and molecular ring cannot be separated although each component is not covalently linked. Based on this structural characteristic, rotaxane combines both static and dynamic properties. As the static property, the molecular ring can strongly and accurately bind to the molecular axle by encircling it. In contrast, the molecular ring can freely move on the molecular axle when the interactions between these components are cleaved. In nature, for example, toroidal processive enzymes, such as DNA polymerase and exonuclease, form a rotaxane-like structure with the target DNA (1). These enzymes enable the accurate recognition of the substrate and the expression of the efficient enzymatic function by taking advantage of both the static and dynamic properties of the rotaxane-like structure (2).

By utilizing the properties of the rotaxane structure, various types of artificial molecular machines have been developed (3,4). For example, Leigh's group developed a molecular machine that mimics the sequence-specific peptide synthesis of nature's ribosomes (5,6), and recently, chemically fueled molecular motors and pumps (7,8). In nucleic acid chemistry, interlocked molecular architectures have been studied for DNA nanotechnology (9–23), topological labels (24–27) and stabilization of the complex (28–31). In addition to the general enzymatic method, a variety of chemical methods that requires a chemical reagent or photoirradiation to construct the interlocked structures have been developed to expand the application.

To further expand the unique properties of the rotaxane into the chemical biology field, a spontaneous rotaxane formation method with the target would be ideal. For example, a functional nucleic acid, which can spontaneously form the rotaxane-like structure with mRNA, might tightly bind to mRNA and strongly inhibit the translation reaction using the static property of the rotaxane. Also, such a functional nucleic acid would create a new method to one-dimensionally move the DNA ring on the target nucleic acids using the dynamic property of the rotaxane, leading to a new tool for a molecular machine and a dynamic DNA/RNA nanotechnology which enables operations even inside the cells.

*To whom correspondence should be addressed. Tel: +81 22 217 5634; Fax: +81 22 217 5633; Email: nagatugi@tagen.tohoku.ac.jp
Correspondence may also be addressed to Kazumitsu Onizuka. Tel: +81 22 217 5634; Fax: +81 22 217 5633; Email: onizuka@tohoku.ac.jp
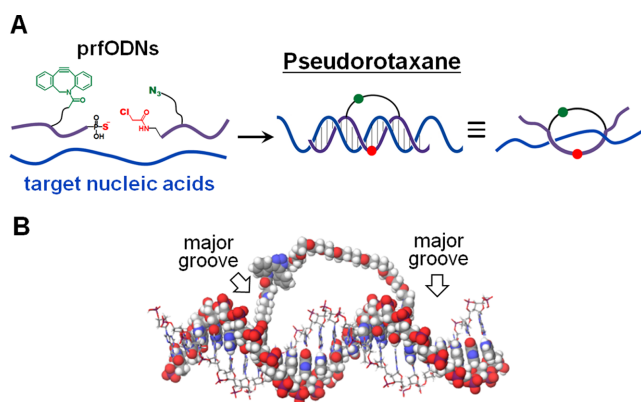
Figure 1. The original pseudorotaxane formation. (**A**) Schematic representation of the pseudorotaxane formaton with the prfODNs. (**B**) Model of the pseudorotaxane structure calculated using the MacroModel software. The linker is linked on the major groove side.

In our previous research, we developed a pair of pseudorotaxane forming oligo DNAs (prfODNs) which spontaneously forms the pseudorotaxane structure with the target nucleic acids (Figure 1) (32). When these prfODNs hybridize with the DNA or RNA target at the same time and at the proper position, an $S_N 2$ type chemical ligation reaction between the phosphorothioate and chloroacetoamide groups occurs. Copper-free click chemistry (33,34) between dibenzylcyclooctyne (DBCO) and an azide group then occurs across a helical turn to provide the pseudorotaxane structure. In this design, prfODNs could successfully form the pseudorotaxane structure, but the reaction yield reached a plateau at 80% for DNA and 70% for RNA. In this study, we attempted the structural optimization of prfODNs to improve the reaction yields, especially for RNA. Additionally, we investigated the relationship between the stability and the ring size of the pseudorotaxane structure.

MATERIALS AND METHODS

The general chemicals were purchased from Wako Pure Chemical, the Tokyo Chemical Institute (TCI), Aldrich, Nacalai Tesque or Kanto Kagaku. The phosphoramidites and CPGs for the DNA synthesis were purchased from the Glen Research or ChemGenes Corporation. The target oligo DNAs and RNAs were purchased from JBioS (Japan). The oligo sequences used in this study are shown in Table 1. The HPLC purification was performed by a JASCO HPLC System (PU-2089Plus, UV-2075Plus and CO-2067Plus) using a reverse-phase C_{18} column (CAP-CELL PAK C18 MGII, Shiseido, 4.6 × 250 mm or 10 × 250 mm). MALDI-TOF MS measurements were performed by a Bruker Autoflex speed instrument using a 3-hydroxypicolinic acid/diammonium hydrogen citrate matrix. The gel imaging and quantification were performed by a FLA-5100 (Fujifilm Co.).

General procedure for pseudorotaxane formation reaction with a pair of prfODNs

A solution (5 μl) of prfODN1′ (1.5 μM), prfODN2 (3 μM) and the target ODN9(with T9 stoppers) or ORN1(with

Table 1. ODN and ORN sequences used in this study

entry	sequences (5'-3') [a, b]
ODN1	TTGCGTTG**X**GC-S (**X** = C[b] or C[s], R[1])
ODN2	TTGCGT**X**GCGC-S (**X** = T[b] or U[s], R[1])
ODN3	TTGCG**X**TGCGC-S (**X** = T[b] or U[s], R[1])
ODN4	TTG**X**GTTGCGC-S (**X** = C[b] or C[s], R[1])
ODN5	**Z**CAC**Y**GCCCGC (**Y** = T[b] or U[s], R[2], **Z** = T, R[3])
ODN6	**Z**CA**Y**TGCCCGC (**Y** = C[s], R[2], **Z** = T, R[3])
ODN7	**Z**C**Y**CTGCCCGC (**Y** = A[s], R[2], **Z** = T, R[3])
ODN8	**ZY**ACGCCCGC (**Y** = C[s], R[2], **Z** = T, R[3])
ODN9	S-AAA<u>GCGGGCAGTGAGCGCAACGCAA</u>TTA-S
ODN10	FAM-TTTT**X**TTTT (**X** = T[b], R[1])
ODN11	FAM-AAA<u>GCGGGCAGTGAGCGCAACGCAA</u>TTA
ODN12	AAA<u>GCGGGCAGTGAGCGCAACGCAA</u>TTA
ODN13	FAM-TTTTAGCTAGCTAGCTAAA<u>GCGGGCAGTGAGCGCAACGCAA</u>TTAAGCTAGCTAGCTTTTT
ODN14	TTGCGTTGCGCTCACTGCCCGC
ODN15	FAM-AAA<u>GCGGG**X**AGTGAGCGC**Y**ACGCAA</u>TTA (**X** = C[s], R[1], **Y** = A[s], R[2])
ORN1	S-AAA<u>gcgggcagugagcgcaacgcaa</u>TTA-S
ORN2	FAM-aaa<u>gcgggcagugagcgcaacgcaa</u>uua
ORN3	FAM-uuuuagcuagcuagcuaaa<u>gcgggcagugagcgcaacgcaa</u>uuaagcuagcuagcuuuuu
ORN4	aaa<u>gcgggcagugagcgcaacgcaa</u>uua

[a] The underline shows the complimentary sequence of the prfODNs.
[b] The capital and small letters denote the DNA and RNA bases, respectively.

T9 stoppers) (1.0 μM) in phosphate buffer (20 mM, pH 7.2) containing NaCl (100 mM), $MgCl_2$ (10 mM) and glutathione (1 mM) was incubated at 37°C. Aliquots of the mixture (2.0 μl each) were removed at 5 min and 60 min, quenched by a loading buffer (80% formamide, 10 mM EDTA, 2.0 μl), then rapidly cooled to 0°C. The samples were analyzed by 16.4% denaturing PAGE (6.2 M urea, 1 × TBE, 18% formamide; 200 V, 60 min, 4 to 15°C) for the target DNA or 15% denaturing PAGE (5.6 M urea, 1 × TBE, 25% formamide; 200V, 60 min, 15°C) for the target RNA.

Determination of dissociation rate constants (k_{off}) of cyODN

A solution (5 μl) of prfODN1′ (1.5 μM), prfODN2 (3 μM) and the target ODN11, ODN9(with T9 stoppers), ODN13 or ORN2 (1.0 μM) in phosphate buffer (20 mM, pH 7.2) containing NaCl (100 mM) and glutathione (1 mM) was incubated at 37°C for 60 min. The mixture was then diluted with a solution (15 μl) of the non-labeled ODN12 or ORN4 target in phosphate buffer containing NaCl and glutathione. The diluted solution (20 μl) of the pseudorotaxane (<0.25 μM) and non-labeled target (5 μM) was incubated at 65°C. Aliquots (2.0 μl each) were removed from the reaction mixture at various time points and quenched by loading buffer (80% formamide, 10 mM EDTA, 2.0 μl), then rapidly cooled to 0°C. The samples were analyzed by 16.4% denaturing PAGE (6.2 M urea, 1 × TBE, 18% formamide; 200 V, 60 min, 4–15°C) for the target DNA or 15% denaturing PAGE (5.6 M urea, 1 × TBE, 25% formamide; 200V, 60 min, 15°C) for the target RNA. The first-order rate constant of the dissociation (k_{off}) was graphically obtained from the first-order kinetic plot (Equation 1). The k_{off} values were determined from three separate experiments.

$$\ln([\text{pseudorotaxane}]_t/[\text{pseudorotaxane}]_0) = -k_{off} \cdot t \quad (1)$$

Melting temperature (T_m) measurement

A solution (82.5 μl) of prfODN1′ (0.75 μM), prfODN2 (1.5 μM) and the target ODN11 or ORN2 (1.0 μM) in phosphate buffer (20 mM, pH 7.2) containing NaCl (100 mM) and DTT (40 μM) was incubated at 37°C for 60 min. The mixture was then diluted with a buffer solution (247.5 μl) containing NaCl. The diluted solution (330 μl) of the pseudorotaxane (<0.25 μM) in phosphate buffer (20 mM, pH 7.2) containing NaCl (100 mM) and DTT (10 μM) was transferred to a microquartz cell with a 1-cm path length. The melting temperature was then measured under UV absorption at 260 nm from 25°C to 95°C at the rate of 1°C/min. The T_m values were determined from two separate experiments. The melting temperature measurement was performed by a DU-800 (Beckman-Coulter) equipped with a temperature controller.

Catenane formation reaction with the cyclized target DNA

A solution (5 μl) of prfODN1′[ODN2 (X = T^b, DBCO; S-S)] (1.5 μM), prfODN2[ODN5(Y = T^s, N$_3$ linker n = 11, Z = T, ClAc)] (3 μM) and the target ODN11 or cyODN15 (1.0 μM) in phosphate buffer (20 mM, pH 7.2) containing NaCl (100 mM), MgCl$_2$ (10 mM) and glutathione (1 mM) was incubated at 37°C for 60 min. The mixture was then diluted with a solution (15 μl) of the non-labeled target ODN12 in phosphate buffer containing NaCl and glutathione. The diluted solution (20 μl) of the pseudorotaxane (<0.25 μM) and non-labeled target (5 μM) was heated at 80°C for 5 min or 10 min. Aliquots (2.0 μl each) were removed from the reaction mixture and quenched by loading buffer (80% formamide, 10 mM EDTA, 2.0 μl), then rapidly cooled to 0°C. The samples were analyzed by 16.4% denaturing PAGE (6.2 M urea, 1 × TBE, 18% formamide; 200 V, 60 min, 4–15°C).

RESULTS AND DISCUSSION

Molecular design and synthesis of prfODNs

To systematically investigate the efficient pseudorotaxane formation reaction, we redesigned the prfODNs in terms of the following three points: the structure of the modified nucleotides (X and Y), the length of the linker (n) and the distance between the modified nucleotides (m) (Figure 2). As for the structure of the modified nucleotides, we designed a sugar-modified nucleotide (U^s or C^s) which has a linker on the minor groove in the duplex in addition to the previous nucleobase-modified nucleotide (T^b or C^b) which has a linker on the major groove (Figure 3) (32). Since the position of the reactive groups (DBCO and N$_3$) on the duplex is important for the template reaction (35), we investigated the minor-minor, major-minor and minor-major combinations (Figure 2C) in addition to the previous major-major combination (Figure 1B). For the length of the PEG linker, we designed the shorter linker with n = 5, 7 and 9 in addition to the previous linker with n = 11. For the distance between the modified nucleotides, we designed m = 8 and 13 in addition to the previous distances m = 10 and 11 by shifting the X position (Figure 2B). Additionally, we designed prfODN1′ protected as a disulfide to prevent the reaction between DBCO and a phosphorothioate because the thiol-yne reaction between a strained alkyne and a thiol has been

reported. The prfODN1′ was expected to be easily deprotected with glutathione and generate prfODN1.

The prfODN1′ was synthesized via ODN1–4 (X, R^1 = H, SS) which were prepared by activating the thioate of ODN1–4 (X, R^1 = H) with 2,2′-dipyridyl disulfide (Supplementary Figure S1). The disulfide product was obtained in high yield using 50% acetonitrile as the solvent in the presence of MgCl$_2$ (50 mM) (Supplementary Figure S2). DBCO modification of ODN1–4 (X, R^1 = H, SS) was carried out using the DBCO NHS ester under alkaline conditions to provide the prfODN1′. The prfODN2 was synthesized from ODN5–8 (Y, R^2 = alkyne, Z = T, R^3 = H) through the copper-catalyzed click reaction (Supplementary Figure S3) (36,37). These ODNs were purified by reversed-phase HPLC and characterized by MALDI-TOF MS measurements (Supplementary Table S1).
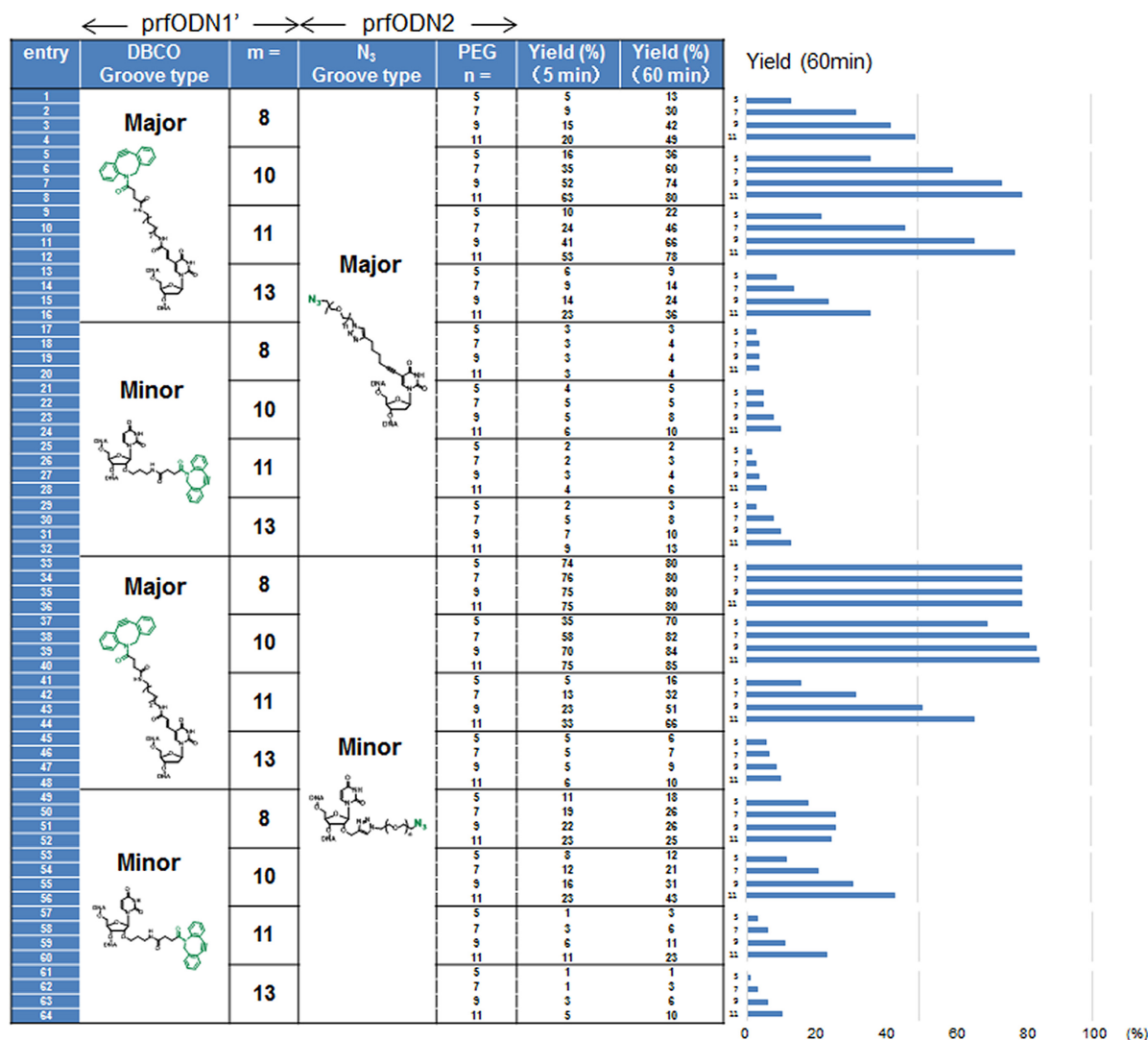
We next designed the target DNA and RNA with two T9 stoppers (thymidine 9 mer ODN10s) to prevent the de-threading of the cyclized ODN during a gel shift assay (Figure 2A). Since the threading of the cyclized ODN via a slippage process becomes slow by the stoppers, the accurate reaction efficiency is expected to be observed (38). The targets with T9 stoppers were synthesized by mixing ODN10 (X = T^b, R^1 = IAc) with ODN9 or ORN1 (Supplementary Figure S4) and labeled with FAM by this modification.

Pseudorotaxane formation reaction

Using the designed prfODN1′, prfODN2 and the target with T9 stoppers, the pseudorotaxane formation reactions were carried out in the presence of glutathione. The reactions were investigated by a denaturing polyacrylamide gel electrophoresis (PAGE) analysis. In Figure 4, ODN2 (X = T^b, DBCO, SS) and ODN5(Y = U^s, N$_3$ linker n = 5, 7, 9 or 11, Z = T, ClAc) were used as the prfODN1′ and prfODN2, respectively. Compared to the band of the target DNA with T9 stoppers, one new clear band indicating the pseudorotaxane structure was observed. The percentage of the complex increased with time. For the reaction with the non-azide-modified ODN5 (Y = U^s, alkyne, Z = T, ClAc), the band of the complex was absent, because no linkage across a helical turn was formed.

We systematically carried out the pseudorotaxane formation reactions regarding all combinations between the prfODN1 and prfODN2, and summarized the relationship between the structure and yield in Figure 5 for the target DNA and Figure 6 for the target RNA. The reaction yields after 5 and 60 min are shown in the table, and the bar graph indicates the yields after 60 min. Compared to the previous result using a pair of major groove type prfODNs, in Figure 5, we found that the yield and efficiency were improved in the combination with the major groove type for prfODN1 and the minor groove type for prfODN2 (entries 33–40). The best yield was 75% in 5 min and 85% in 60 min using prfODN1 (major, m = 10) and prfODN2 (minor, n = 11) (entry 40). On the other hand, the yields were significantly low for the minor-major combination (entries 17–32). As for the target RNA, similar to the DNA target, we found an improved yield and efficiency for the combination with the major groove type for prfODN1 and the minor groove type for prfODN2 (Figure 6, entries 33–44). The best yield

Figure 2. Molecular design to optimize prfODNs. (**A**) Schematic representation of the pseudorotaxane formaton with the designed prfODNs. PrfODN1′ can produce prfODN1 by the S-S bond cleavage with glutathione. (**B**) Sequences of the prfODNs. M indicates the base number from Y to X. (**C**) The model of the DNA/DNA duplex structure was calculated using the MacroModel software. The DBCO and azide groups are placed on either the major or minor groove.

Figure 3. Structures of modified nucleotide.

Figure 4. Gel image of pseudorotaxane formaton using the prfODNs and target DNA. The reaction was carried out with ODN2 (X = T^b, DBCO, SS) (1.5 μM), ODN5(Y = U^s, N_3 linker n = 5, 7, 9 or 11, Z = T, ClAc) (3.0 μM) and target ODN9(with T9 stoppers) (1.0 μM) in phosphate buffer (20 mM, pH 7.2) containing NaCl (100 mM), $MgCl_2$ (10 mM) and glutathione (1 mM) at 37°C for 5 or 60 min. The electrophoresis was performed at 15°C on a 16.4% denaturing polyacrylamide gel containing 18% formamide.

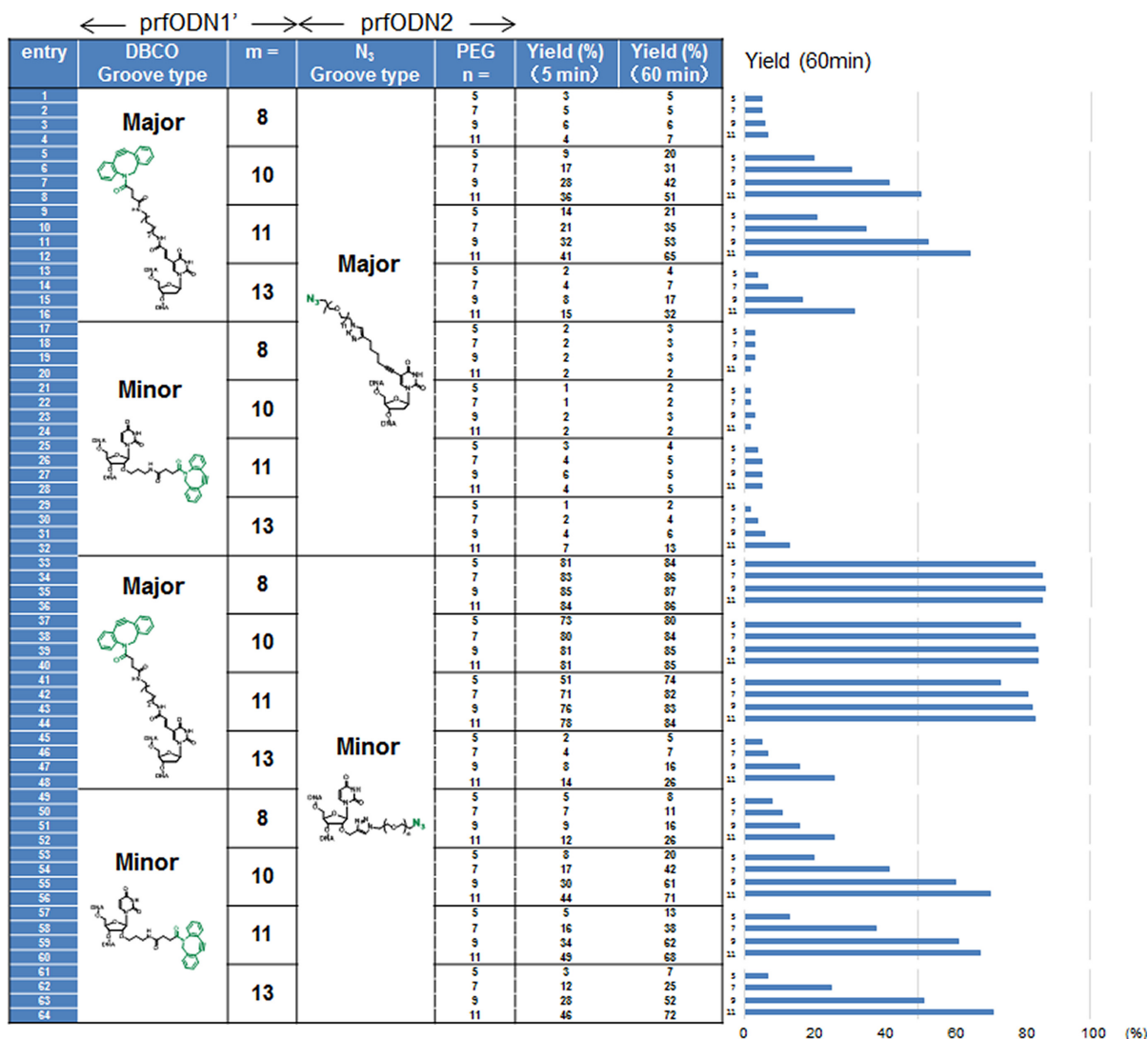|	← prfODN1' →		← prfODN2 →				Yield (60min)
entry	DBCO Groove type	m =	N₃ Groove type	PEG n =	Yield (%) (5 min)	Yield (%) (60 min)	
1	Major	8	Major	5	5	13	
2				7	9	30	
3				9	15	42	
4				11	20	49	
5		10		5	16	36	
6				7	35	60	
7				9	52	74	
8				11	63	80	
9		11		5	10	22	
10				7	24	46	
11				9	41	66	
12				11	53	78	
13		13		5	6	9	
14				7	9	14	
15				9	14	24	
16				11	23	36	
17	Minor	8		5	3	3	
18				7	3	4	
19				9	3	4	
20				11	3	4	
21		10		5	4	5	
22				7	5	5	
23				9	5	8	
24				11	6	10	
25		11		5	2	2	
26				7	2	3	
27				9	3	4	
28				11	4	6	
29		13		5	2	3	
30				7	5	8	
31				9	7	10	
32				11	9	13	
33	Major	8	Minor	5	74	80	
34				7	76	80	
35				9	75	80	
36				11	75	80	
37		10		5	35	70	
38				7	58	82	
39				9	70	84	
40				11	75	85	
41		11		5	5	16	
42				7	13	32	
43				9	23	51	
44				11	33	66	
45		13		5	5	6	
46				7	5	7	
47				9	5	9	
48				11	6	10	
49	Minor	8		5	11	18	
50				7	19	26	
51				9	22	26	
52				11	23	25	
53		10		5	8	12	
54				7	12	21	
55				9	16	31	
56				11	23	43	
57		11		5	1	3	
58				7	3	6	
59				9	6	11	
60				11	11	23	
61		13		5	1	1	
62				7	1	3	
63				9	3	6	
64				11	5	10	

Figure 5 Pseudorotaxane formaton using the prfODNs and target DNA. The reaction was carried out with prfODN1′ (1.5 μM), prfODN2 (3.0 μM) and target ODN9(with T9 stoppers) (1.0 μM) in phosphate buffer (20 mM, pH 7.2) containing NaCl (100 mM), MgCl₂ (10 mM) and glutathione (1 mM) at 37°C for 5 or 60 min. The blue bar graph indicates the reaction yields in 60 min.

was 87% after 60 min, and even after 5 min, the yield was 85% using prfODN1 (major, $m = 8$) and prfODN2 (minor, $n = 9$) (entry 35). For the minor-major combination (entries 17–32), the yields were significantly low as well as the target DNA.

The model structures of the DNA–DNA and DNA–RNA duplexes are shown in Figure 7A and B. In the case of the previous major-major combination, reactive groups for the click reaction have to cross over the minor groove because the threaded structure is not formed when the linkers are linked along the major groove. The same applies to the case of the minor-minor combination. On the other hand, in the case of the major-minor combination, the yield and efficiency increased because the reactive groups can react with each other by the shortest distance (Figure 7C). In addition, the high yield of the major-minor combination might be because the linkers are not linked along the major or minor groove. For the minor-major combination, the reaction did

not proceed because the reactive groups were far away from each other (Figure 7D). When comparing the DNA target with RNA target, the yields of the DNA target were higher in the major-major combinations but lower in the minor-minor combinations than RNA target (Figures 5 and 6). For DNA target, B-form duplex was formed from the CD spectra (Supplementary Figure S5A) and the model (Figure 7A). For RNA target, A-form duplex was formed (Supplementary Figure S5B and Figure 7B). Generally, B-form duplex has a wide major groove and a narrow minor groove (Figure 7A). In contrast, A-form duplex has a narrow major groove and a wide minor groove (Figure 7B). When the intersected groove was narrower, the higher yields of the pseudorotaxane formation were observed (major-major > minor-minor in the DNA target; major-major < minor-minor in the RNA target). In addition, when the long distance $m = 13$ was used, the yields significantly decreased, especially in the major-minor combination (entries 45–48)

entry	prfODN1' DBCO Groove type	m =	prfODN2 N3 Groove type	PEG n =	Yield (%) (5 min)	Yield (%) (60 min)
1	Major	8	Major	5	3	5
2				7	5	5
3				9	6	6
4				11	4	7
5		10		5	9	20
6				7	17	31
7				9	28	42
8				11	36	51
9		11		5	14	21
10				7	21	35
11				9	32	53
12				11	41	65
13		13		5	2	4
14				7	4	7
15				9	8	17
16				11	15	32
17	Minor	8		5	2	3
18				7	2	3
19				9	2	3
20				11	2	2
21		10		5	1	2
22				7	1	2
23				9	2	3
24				11	2	2
25		11		5	3	4
26				7	4	5
27				9	6	5
28				11	4	5
29		13		5	1	2
30				7	2	4
31				9	4	6
32				11	7	13
33	Major	8	Minor	5	81	84
34				7	83	86
35				9	85	87
36				11	84	86
37		10		5	73	80
38				7	80	84
39				9	81	85
40				11	81	85
41		11		5	51	74
42				7	71	82
43				9	76	83
44				11	78	84
45		13		5	2	5
46				7	4	7
47				9	8	16
48				11	14	26
49	Minor	8		5	5	8
50				7	7	11
51				9	9	16
52				11	12	26
53		10		5	8	20
54				7	17	42
55				9	30	61
56				11	44	71
57		11		5	5	13
58				7	16	38
59				9	34	62
60				11	49	68
61		13		5	3	7
62				7	12	25
63				9	28	52
64				11	46	72

Figure 6 Pseudorotaxane formaton using the prfODNs and target RNA. The reaction was carried out with prfODN1' (1.5 μM), prfODN2 (3.0 μM) and target ORN1 (with T9 stoppers) (1.0 μM) in phosphate buffer (20 mM, pH 7.2) containing NaCl (100 mM), MgCl$_2$ (10 mM) and glutathione (1 mM) at 37°C for 5 or 60 min. The blue bar graph indicates the reaction yields in 60 min.

probably due to the mismatch direction of the linker in addition to the long distance. These results suggest that the yields of the pseudorotaxane formation would be affected by the distance between the reactive groups, the width of the intersected groove and the linker direction.

We next focused on the PEG linker length. In Figures 5 and 6, only the major-minor combination showed high yields when a short PEG linker ($n = 5$) was used because the reactive groups can react in a short distance. For the other combinations, the yield drastically decreased as a linker gets shorter. Also, for the distance between the modified nucleotides (m), only the major-minor combination showed high yields when the short distance m = 8 was used. Thus, the pseudorotaxane structure with the small ring can be formed only using the major-minor combination. We next investigated the pseudorotaxane formation with a smaller ring using prfODN1 (major, $m = 5$–8), prfODN2 (minor, $n = 3$ or 5) and target ORN1 (with T9

stoppers) (Supplementary Figure S6). The yields of all combinations in Supplementary Figure S6 were lower than that of the prfODN1 (major, $m = 8$) and prfODN2 (minor, $n = 5$) combination. The $n = 3$ linker would be too short and the distance ($m = 5$–7) would be unfavorable for the reaction.

Kinetic and thermal stability of pseudorotaxane structures

Since we considered that a smaller ring size would form a more stable pseudorotaxane complex, we investigated the correlation between the ring size and the kinetic and thermal stabilities. The investigation of the kinetic stability was performed by measuring the half-life of pseudorotaxane during the dethreading reaction. After the pseudorotaxane formation reaction with prfODN1' and prfODN2, the pseudorotaxane structure was heated at 65°C and the dethreaded cyclized ODN (cyODN) was trapped with the non-labeled target ODN14 or ORN4 to prevent the pseudorotaxane reformation via the slippage process which we
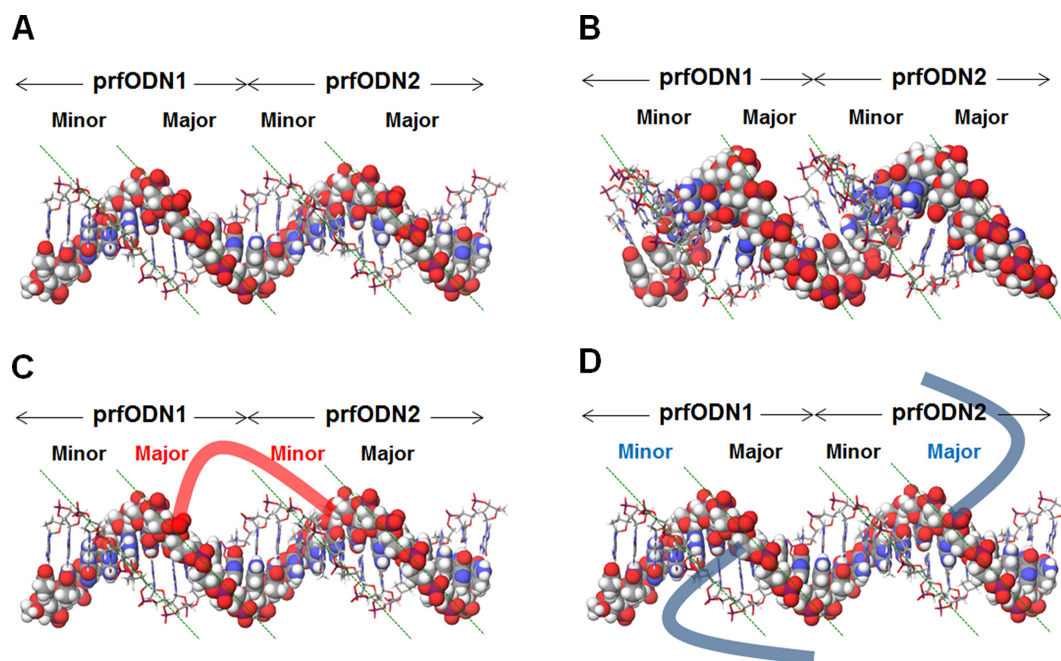
Figure 7. Schematic for the discussion of pseudorotaxane formation reaction with different groove type prfODNs. (**A**) DNA–DNA duplex. (**B**) DNA–RNA duplex. (**C**) Major–minor combination. (**D**) Minor–major combination. The models were calculated using the MacroModel software. The prfODNs are shown as the CPK model.

previously reported (Figure 8A) (38). Based on the gel shift assay, the first-order reaction rate of the dethreading and its half-life ($t_{1/2}$) were calculated (Figure 8B–D). Table 2 shows the pseudorotaxane formation yields, dethreading rates (k_{off}), half-lives and T_m values. As for the DNA target, the half-life of the major-major combination ($m = 10$, $n = 11$ or 7) was short (6.5 min or 9.1 min) (entries 1 and 2). In contrast, when the minor-minor or major-minor combination ($m = 10$, $n = 11$) was used, a relatively long half-life of 63 and 58 min was observed (entries 3 and 4). For the major-minor combination, the half-life increased with a decrease in the linker length (n) and the distance between the modified nucleotides (m) (entries 5–7). Interestingly, using a stoppered ODN**9** or longer target ODN**13**, the half-life drastically increased because the distance to dethread got longer (entries 8 and 9). This dethreading distance-dependent stabilization will be the unique property of the pseudorotaxane structure. We next measured the T_m values to investigate the thermal stability. For the major-minor combination, the T_m values also increased with a decrease in the ring size. Compared to the canonical duplex (entry 10), the pseudorotaxane structures of the major-minor combination were kinetically more stable, but not thermally more stable. The pseudorotaxane structures would be kinetically stabilized by the restriction of the structure changes, in contrast, the thermal stability would decrease probably due to the small disturbance in the duplex structure resulting from the linkage (38). As for the major-major combination, both the kinetic and thermal stabilities significantly decreased. This destabilization would be due to the larger disturbance in the duplex structure resulting from the direct linkage of the nucleobases which is important for the hydrogen bond formation. However, this combination would be useful when we take

advantage of the dynamic property of the pseudorotaxane such as the creation of a molecular machine.

For the RNA target, a result similar to the DNA target was observed. The half-life of the major-major combination ($m = 10$, $n = 11$) was short (24 min) (entry 11). For the minor-minor combination ($m = 10$, $n = 11$), the long half-life of 403 min was observed (entry 12). For the major-minor combination, the half-life increased with a decrease in the linker length (n) and the distance between the modified nucleotides (m) (entry 13–16). Especially, the psudorotaxane structure of entry 16 ($m = 8$, $n = 5$) was both kinetically and thermally more stable than the canonical duplex (entry 17). This combination (entry 16) also showed an excellent yield for the pseudorotaxane formation reaction. In Figure 9, we showed the model structure of this combination. This linkage would not disturb the duplex structure even though the linker length is short, leading to the stable complex formation and efficient reaction. This combination will be the best when we utilize the static property of the pseudorotaxane. These prfODNs would form a stable complex with the mRNA and might significantly inhibit the translation and splicing reaction for a similar type of antisense oligonucleotide with cross-linking oligonucleotides (39).

Catenane formation reaction

To verify the threaded structure of the pseudorotaxane formed by the major-minor combination, we attempted the catenane formation using the chemically cyclized DNA (cyDNA) target. Since each ring of the catenane structure cannot be separated without bond cleavage, the threaded structure should be stable even under high temperature conditions. The cyDNA target was prepared by the in-
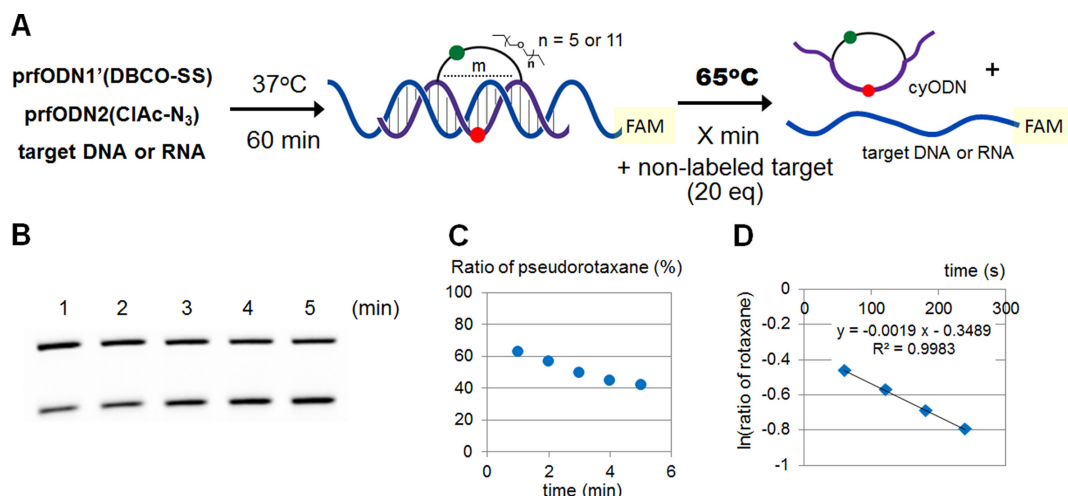
Figure 8. Kinetic stability of the pseudorotaxane structure. (**A**) Schematic representation of the pseudorotaxane formation and dissociation. The dissociation rate constant (k_{off}) of cyODNs formed by pseudorotaxane formation reaction was calculated. First, the pseudorotaxane structure was formed with prfODN1′ (1.5 μM), prfODN2 (3.0 μM) and target ODN11 or ORN2 (1.0 μM) in phosphate buffer (20 mM, pH 7.2) containing NaCl (100 mM) and glutathione (1 mM) at 37°C for 60 min. The dissociation of cyODN was then performed with the pseudorotaxane (<0.25 μM) and non-labeled target ODN12 or ORN4 (5.0 μM) in the same buffer at 65°C. (**B**) Gel image of the DNA–DNA pseudorotaxane structure formed by prfODN1 (major, $m = 10$) and prfODN2 (major, $n = 11$) and its dissociation. (**C**) Ratio of the pseudorotaxane structure on the gel image in B. (**D**) Calculation of the dissociation rate constant (k_{off}) of the cyODN formed by prfODN1 (major, $m = 10$) and prfODN2 (major, $n = 11$).

Table 2. Kinetic and thermal stability of pseudorotaxane

Entry	Target	DBCO groove type	$m =$	N_3 groove type	Linker ($n =$)	Formation yield (%) [a]	k_{off} (s^{-1}) [b]	$t_{1/2}$ (min)	T_m (°C) [c]
1	ODN11	Major	10	Major	11	80	1.8×10^{-3}	6.5	70.5 (-9.2)
2	ODN11	Major	10	Major	7	60	1.3×10^{-3}	9.1	- [d]
3	ODN11	Minor	10	Minor	11	43	1.8×10^{-4}	63	- [d]
4	ODN11	Major	10	Minor	11	85	2.0×10^{-4}	58	72.4 (-7.3)
5	ODN11	Major	10	Minor	5	70	9.1×10^{-5}	127	72.6 (-7.1)
6	ODN11	Major	8	Minor	11	80	1.2×10^{-4}	94	75.0 (-4.7)
7	ODN11	Major	8	Minor	5	80	5.4×10^{-5}	214	76.9 (-2.8)
8	stopper [e]	Major	8	Minor	5	80	1.9×10^{-5}	608	- [f]
9	ODN13	Major	8	Minor	5	80	9.2×10^{-6}	1260	- [f]
10	ODN11	(ODN14)	-	-	-	-	1.4×10^{-4}	83	79.7
11	ORN2	Major	10	Major	11	51	4.8×10^{-4}	24	71.3 (-9.0)
12	ORN2	Minor	10	Minor	11	71	2.9×10^{-5}	403	77.5 (-2.8)
13	ORN2	Major	10	Minor	11	85	3.2×10^{-5}	361	78.2 (-2.1)
14	ORN2	Major	10	Minor	5	80	2.2×10^{-5}	517	79.3 (-1.0)
15	ORN2	Major	8	Minor	11	86	3.2×10^{-5}	365	80.1 (-0.2)
16	ORN2	Major	8	Minor	5	84	1.6×10^{-5}	722	82.3 (+2.0)
17	ORN2	(ODN14)	-	-	-	-	2.1×10^{-4}	56	80.3

[a]The yields after 60 min from Figure 5 or 6.
[b]Error < 17%.
[c]The T_m values were measured using pseudorotaxane (< 0.25 μM) in phosphate buffer (20 mM, pH 7.2) containing NaCl (100 mM) and DTT (10 μM). The number in parentheses shows the difference between the pseudorotaxane and native duplex.
[d]The T_m value could not be clearly calculated due to the low pseudorotaxane formation yield.
[e]Target ODN9 (with T9 stoppers).
[f]The T_m value could not be calculated.

tramolecular Cu-catalyzed click reaction of ODN15 (X = C^s, propargyl, Y = A^s, N_3 linker) (Supplementary Figure S7). The catenane formation reaction was performed with prfODN1′ (major, m = 10), prfODN2 (minor, n = 11) and cyODN15 (cyDNA target) at 37°C for 60 min. The product was then heated at 80°C for 5 and 10 min in the presence of the non-labeled target ODN12 which traps prfODN1′, prfODN2 and their non-threaded products (Figure 10A). As the control experiment, the pseudorotaxane formation was carried out with the linear target ODN11. While the complex consisting of the linear target DNA rapidly disappeared by heating, the complex consisting of the cyDNA was stable to heating at 80°C for 10 min (Figure 10B, C). The complex consisting of the cyDNA was extracted from gels and the molecular weight was analyzed by a MALDI-TOF MS measurement. The clear peak corresponding to the molecular weight of the catenane complex was observed (Supplementary Figure S8). In addition, prfODN1′
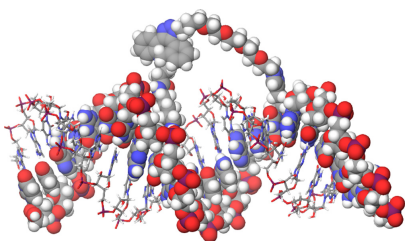
Figure 9. The model of the DNA–RNA pseudorotaxane structure formed by prfODN**1** (major, $m = 8$) and prfODN**2** (minor, $n = 5$). The model was calculated using the MacroModel software with the OPLS_2005 force field. The prfODN is shown as the CPK model.
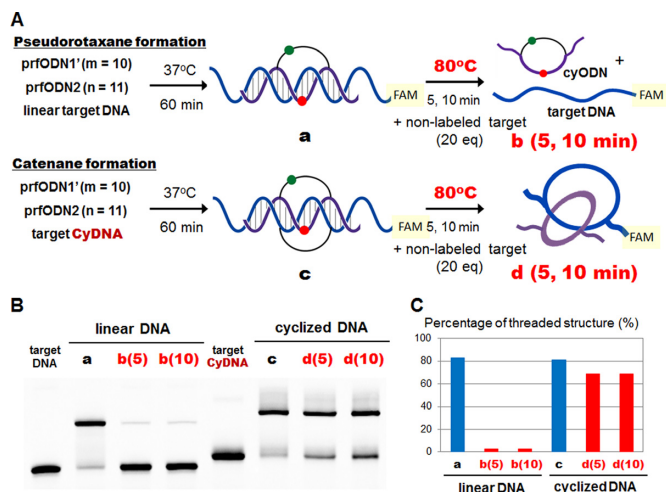
Figure 10. Catenane formation with the cyclized target DNA. (**A**) Schematic representation of the pseudorotaxane and catenane formation. The pseudorotaxane or catenane formation was performed with prfODN**1**′ (major, $m = 10$) (1.5 μM), prfODN**2** (minor, $n = 11$) (3.0 μM) and target ODN**11** or cyODN**15** (1.0 μM) in phosphate buffer (20 mM, pH 7.2) containing NaCl (100 mM), MgCl$_2$ (10 mM) and glutathione (1 mM) at 37°C for 60 min (sample **a** or **c**). The non-labeled target ODN**12** (20 eq) was added and the mixture was heated at 80°C for 5 or 10 min (**b** or **d**). The electrophoresis was performed at 4–15°C on a 16.4% denaturing polyacrylamide gel containing 18% formamide. (**B**) Gel image of the pseudorotaxane formation using the linear DNA and catenane formation using the cyclized DNA. (**C**) Percentage of the threaded structure (upper band) on the gel image in B.

or prfODN**2** did not directly react with the cyDNA target (Supplementary Figure S9). These results clearly indicated that the complex consisting of the cyDNA is the catenane structure and the prfODNs of the major-minor combination form the threaded structure.

CONCLUSIONS

We have described the structural optimization of prfODNs for the efficient and stable complex formation. During the systematic investigation of the pseudorotaxane formation reaction, we found that the major-minor combination showed a high yield and efficiency because the reactive groups can successfully approach each other. This finding would be valuable information for the development of nucleic acids templated reactions (35,40). In this investigation, the pseudorotaxane structure with the smaller ring size

was efficiently formed only using the major-minor combination. Especially, the psudorotaxane structure (major-minor, $m = 8$, $n = 5$) was kinetically and thermally more stable than the others. Since the other combinations did not provide the pseudorotaxane structure with such a short ring ($m = 8$, $n = 5$) and stable complex, the major-minor combination will be the best to take advantage of the static property of the pseudorotaxane structure. In contrast, the pseudorotaxane structure with the major–major combination decreased both the kinetic and thermal stabilities. This combination would be useful to utilize the dynamic property of the pseudorotaxane structure. The incorporation of the photo-response moieties, such as the azobenzene derivatives (12,41) or o-nitorobenzyl derivatives (42,43) into the prfODNs, will provide the photo-response movable function to the cyclized ODN, and their prfODNs will be a novel tool for dynamic DNA/RNA nanotechnology.

To verify the threaded structure of the pseudorotaxane, the catenane formation using the cyDNA was carried out. The catenane formation efficiently proceeded as well as the pseudorotaxane formation with the linear target ODN. The catenane structure was thermally stable and its molecular weight was observed by the MALDI-TOF MS measurement without any component separation. These results provided the conclusive evidence that the prfODNs successfully form a threaded structure such as the pseudorotaxane and catenane structures. This catenane formation as well as pseudorotaxane formation would be a new method to create the interlocked structure.

Both the static and dynamic properties of the rotaxane-like structure are attractive for developing novel functional nucleic acids. The information acquired in this study would lead to the development of novel chemical tools using the prfODNs such as antisense oligonucleotides and a movable DNA ring on a nucleic acid.

SUPPLEMENTARY DATA

Supplementary Data are available at NAR Online.

REFERENCES

1. Breyer,W.A. and Matthews,B.W. (2001) A structural basis for processivity. *Protein Sci.*, **10**, 1699–1711.

2. van Dongen,S.F., Elemans,J.A., Rowan,A.E. and Nolte,R.J. (2014) Processive catalysis. *Angew. Chem. Int. Ed.*, **53**, 11420–11428.

3. Erbas-Cakmak,S., Leigh,D.A., McTernan,C.T. and Nussbaumer,A.L. (2015) Artificial molecular machines. *Chem. Rev.*, **115**, 10081–10206.

4. Cheng,C. and Stoddart,J.F. (2016) Wholly synthetic molecular machines. *ChemPhysChem*, **17**, 1780–1793.

5. Lewandowski,B., De Bo,G., Ward,J.W., Papmeyer,M., Kuschel,S., Aldegunde,M.J., Gramlich,P.M., Heckmann,D., Goldup,S.M., D'Souza,D.M. *et al.* (2013) Sequence-specific peptide synthesis by an artificial small-molecule machine. *Science*, **339**, 189–193.

6. De Bo,G., Kuschel,S., Leigh,D.A., Lewandowski,B., Papmeyer,M. and Ward,J.W. (2014) Efficient assembly of threaded molecular machines for sequence-specific synthesis. *J. Am. Chem. Soc.*, **136**, 5811–5814.

7. Wilson,M.R., Sola,J., Carlone,A., Goldup,S.M., Lebrasseur,N. and Leigh,D.A. (2016) An autonomous chemically fuelled small-molecule motor. *Nature*, **534**, 235–240.

8. Erbas-Cakmak,S., Fielden,S.D.P., Karaca,U., Leigh,D.A., McTernan,C.T., Tetlow,D.J. and Wilson,M.R. (2017) Rotary and linear molecular motors driven by pulses of a chemical fuel. *Science*, **358**, 340–343.

9. Kumar,R., El-Sagheer,A., Tumpane,J., Lincoln,P., Wilhelmsson,L.M. and Brown,T. (2007) Template-directed oligonucleotide strand ligation, covalent intramolecular DNA circularization and catenation using click chemistry. *J. Am. Chem. Soc.*, **129**, 6859–6864.

10. Ackermann,D., Schmidt,T.L., Hannam,J.S., Purohit,C.S., Heckel,A. and Famulok,M. (2010) A double-stranded DNA rotaxane. *Nat. Nanotechnol.*, **5**, 436–442.

11. Schmidt,T.L. and Heckel,A. (2011) Construction of a structurally defined double-stranded DNA catenane. *Nano Lett.*, **11**, 1739–1742.

12. Lohmann,F., Ackermann,D. and Famulok,M. (2012) Reversible light switch for macrocycle mobility in a DNA rotaxane. *J. Am. Chem. Soc.*, **134**, 11884–11887.

13. Sannohe,Y. and Sugiyama,H. (2012) Single strand DNA catenane synthesis using the formation of G-quadruplex structure. *Bioorg. Med. Chem.*, **20**, 2030–2034.

14. Ackermann,D. and Famulok,M. (2013) Pseudo-complementary PNA actuators as reversible switches in dynamic DNA nanotechnology. *Nucleic Acids Res.*, **41**, 4729–4739.

15. Liu,X., Lu,C.H. and Willner,I. (2014) Switchable reconfiguration of nucleic acid nanostructures by stimuli-responsive DNA machines. *Acc. Chem. Res.*, **47**, 1673–1680.

16. Li,T., Lohmann,F. and Famulok,M. (2014) Interlocked DNA nanostructures controlled by a reversible logic circuit. *Nat. Commun.*, **5**, 4940.

17. Wu,Z.S., Shen,Z., Tram,K. and Li,Y. (2014) Engineering interlocking DNA rings with weak physical interactions. *Nat. Commun.*, **5**, 4279.

18. Powell,J.T., Akhuetie-Oni,B.O., Zhang,Z. and Lin,C. (2016) DNA origami Rotaxanes: Tailored synthesis and controlled structure switching. *Angew. Chem. Int. Ed.*, **55**, 11412–11416.

19. List,J., Falgenhauer,E., Kopperger,E., Pardatscher,G. and Simmel,F.C. (2016) Long-range movement of large mechanically interlocked DNA nanostructures. *Nat. Commun.*, **7**, 12414.

20. Lu,C.H., Cecconello,A. and Willner,I. (2016) Recent advances in the synthesis and functions of reconfigurable interlocked DNA nanostructures. *J. Am. Chem. Soc.*, **138**, 5172–5185.

21. Weigandt,J., Chung,C.L., Jester,S.S. and Famulok,M. (2016) Daisy chain rotaxanes made from interlocked DNA nanostructures. *Angew. Chem. Int. Ed.*, **55**, 5512–5516.

22. Li,Q., Wu,G., Wu,W. and Liang,X. (2016) Efficient synthesis of topologically linked three-ring DNA catenanes. *ChemBioChem*, **17**, 1127–1131.

23. Centola,M., Valero,J. and Famulok,M. (2017) Allosteric control of oxidative catalysis by a DNA rotaxane nanostructure. *J. Am. Chem. Soc.*, **139**, 16044–16047.

24. Nilsson,M., Malmgren,H., Samiotaki,M., Kwiatkowski,M., Chowdhary,B.P. and Landegren,U. (1994) Padlock probes: circularizing oligonucleotides for localized DNA detection. *Science*, **265**, 2085–2088.

25. Escude,C., Garestier,T. and Helene,C. (1999) Padlock oligonucleotides for duplex DNA based on sequence-specific triple helix formation. *Proc. Natl. Acad. Sci. U.S.A.*, **96**, 10603–10607.

26. Roulon,T., Helene,C. and Escude,C. (2002) Coupling of a targeting peptide to plasmid DNA using a new type of padlock oligonucleotide. *Bioconjugate Chem.*, **13**, 1134–1139.

27. Liu,Y., Kuzuya,A., Sha,R., Guillaume,J., Wang,R., Canary,J.W. and Seeman,N.C. (2008) Coupling across a DNA helical turn yields a hybrid DNA/organic catenane doubly tailed with functional termini. *J. Am. Chem. Soc.*, **130**, 10882–10883.

28. Wang,S. and Kool,E.T. (1994) Circular RNA oligonucleotides. Synthesis, nucleic acid binding properties, and a comparison with circular DNAs. *Nucleic Acids Res.*, **22**, 2326–2333.

29. Ryan,K. and Kool,E.T. (1998) Triplex-directed self-assembly of an artificial sliding clamp on duplex DNA. *Chem. Biol.*, **5**, 59–67.

30. Kool,E.T. (1998) Recognition of DNA, RNA, and proteins by circular oligonucleotides. *Acc. Chem. Res.*, **31**, 502–510.

31. Fujimoto,K., Matsuda,S., Yoshimura,Y., Ami,T. and Saito,I. (2007) Reversible photopadlocking on double-stranded DNA. *Chem. Commun.*, 2968–2970.

32. Onizuka,K., Nagatsugi,F., Ito,Y. and Abe,H. (2014) Automatic pseudorotaxane formation targeting on nucleic acids using a pair of reactive oligodeoxynucleotides. *J. Am. Chem. Soc.*, **136**, 7201–7204.

33. Agard,N.J., Prescher,J.A. and Bertozzi,C.R. (2004) A strain-promoted [3 + 2] azide-alkyne cycloaddition for covalent modification of biomolecules in living systems. *J. Am. Chem. Soc.*, **126**, 15046–15047.

34. Debets,M.F., van Berkel,S.S., Schoffelen,S., Rutjes,F.P., van Hest,J.C. and van Delft,F.L. (2010) Aza-dibenzocyclooctynes for fast and efficient enzyme PEGylation via copper-free (3+2) cycloaddition. *Chem. Commun.*, **46**, 97–99.

35. Gorska,K. and Winssinger,N. (2013) Reactions templated by nucleic acids: more ways to translate oligonucleotide-based instructions into emerging function. *Angew. Chem. Int. Ed.*, **52**, 6820–6843.

36. Gramlich,P.M., Wirges,C.T., Manetto,A. and Carell,T. (2008) Postsynthetic DNA modification through the copper-catalyzed azide-alkyne cycloaddition reaction. *Angew. Chem. Int. Ed.*, **47**, 8350–8358.

37. Su,M., Kirchner,A., Stazzoni,S., Muller,M., Wagner,M., Schroder,A. and Carell,T. (2016) 5-Formylcytosine could be a semipermanent base in specific genome sites. *Angew. Chem. Int. Ed.*, **55**, 11797–11800.

38. Onizuka,K., Chikuni,T., Amemiya,T., Miyashita,T., Onizuka,K., Abe,H. and Nagatsugi,F. (2017) Pseudorotaxane formation via the slippage process with chemically cyclized oligonucleotides. *Nucleic Acids Res.*, **45**, 5036–5047.

39. Nagatsugi,F. and Imoto,S. (2011) Induced cross-linking reactions to target genes using modified oligonucleotides. *Org. Biomol. Chem.*, **9**, 2579–2585.

40. Di Pisa,M. and Seitz,O. (2017) Nucleic acid templated reactions for chemical biology. *ChemMedChem*, **12**, 872–882.

41. Kamiya,Y. and Asanuma,H. (2014) Light-driven DNA nanomachine with a photoresponsive molecular engine. *Acc. Chem. Res.*, **47**, 1663–1672.

42. Ordoukhanian,P. and Taylor,J.-S. (1995) Design and synthesis of a versatile photocleavable DNA building block. Application to phototriggered hybridization. *J. Am. Chem. Soc.*, **117**, 9570–9571.

43. Hausch,F. and Jaschke,A. (2000) Multifunctional DNA conjugates for the in vitro selection of new catalysts. *Nucleic Acids Res.*, **28**, e35.